Nonaxisymmetric Instability of Shear-Banded Taylor-Couette Flow

Alexandre Nicolas[1,2] and Alexander Morozov[1,*]

[1]SUPA, School of Physics & Astronomy, University of Edinburgh, JCMB, King's Buildings, Mayfield Road, EH9 3JZ, Edinburgh, United Kingdom

[2]Ecole Polytechnique, 91128 Palaiseau, France

(Received 15 August 2011; published 22 February 2012)

Recent experiments show that shear-banded flows of semidilute wormlike micelles in Taylor-Couette geometry exhibit a flow instability in the form of Taylor-like vortices. Here we perform the nonaxisymmetric linear stability analysis of the diffusive Johnson-Segalman model of shear banding and show that the nature of this instability depends on the applied shear rate. For the experimentally relevant parameters, we find that at the beginning of the stress plateau the instability is driven by the interface between the bands, while most of the stress plateau is occupied by the bulk instability of the high-shear-rate band. Our work significantly alters the recently proposed stability diagram of shear-banded flows based on axisymmetric analysis.

DOI: 10.1103/PhysRevLett.108.088302 PACS numbers: 83.80.Qr, 47.50.Gj

Flows of complex fluids often differ dramatically from their Newtonian counterparts [1]. One of the most striking examples of such differences is the phenomenon of shear-banding which is widespread in flows of micellar solutions [1,2], granular media [3], foams [4] and colloidal glasses [5]. Its name is derived from the observation that when sheared these materials often split into two or more bands of different shear rates, viscosities and viscoelastic properties [1,2]. In semidilute solutions of wormlike micelles, shear-banding is often associated with the so-called *shear-stress plateau*—the range of applied shear rates $\dot{\gamma}_{\mathrm{app}}$ for which the shear stress Σ is approximately independent of $\dot{\gamma}_{\mathrm{app}}$ [2,6,7]. Outside the stress plateau, simple 1D shear flow remains homogeneous, while for the values of $\dot{\gamma}_{\mathrm{app}}$ on the plateau, it splits into two regions of simple shear flow with different shear rates [2].

Recent experiments with semidilute wormlike micellar solutions have demonstrated that this picture of steady 1D shear-banded flows only holds *on average* [8–11]. Visualization experiments in flows between two rotating coaxial cylinders, the Taylor-Couette flow, have shown that on the stress plateau, there exist large instantaneous fluctuations in local stresses and the local position of the interface between the two bands that are associated with a 3D hydrodynamic instability [8–10]. This instability has the form of doughnut-shaped vortices threaded by the inner cylinder and stacked in the vorticity direction (Taylor-like vortices) and is mainly localized in the high-shear-rate band [11]. Its origin is not inertial due to the low flow velocities and large viscosities involved [2].

Presently, the precise nature of the instability driving the Taylor-like vortices and undulations of the interface remains unclear. Possible mechanisms include an instability driven by the presence of the interface (*interfacial mode*) or a bulk instability inside one or both bands (*bulk mode*). The interfacial mode is a viscoelastic analogue of the Kelvin-Helmholtz instability and arises in coflows of several liquids with a discontinuity in their normal-stress differences across the interface [12]. The bulk mode, which has been observed in Taylor-Couette flow of polymer solutions, is driven by large values of the first normal-stress difference N_1 in the bulk, and the presence of curved streamlines [13,14]. Unlike Newtonian Taylor-Couette flow where the first instability results in an axisymmetric stack of Taylor vortices, linear stability analysis predicts that viscoelastic Taylor-Couette flow is unstable towards nonaxisymmetric (wavy in the azimuthal direction) Taylor-like vortices [15].

Previous attempts to uncover the nature of the instability in the shear-banded Taylor-Couette flow focused on the *axisymmetric* version of this flow [16]. By performing numerical simulations, Fielding has concluded that micellar solutions split into three groups depending on their material properties: fluids with low values of the first normal-stress difference N_1 in their high-shear-rate band exhibit the interfacial instability [15], while fluids with high values of N_1 exhibit the bulk instability in curved geometries [16]. For intermediate values of N_1, the flow was predicted to be stable, and the precise position of this region was found to depend on the curvature of the Taylor-Couette cell [16]. The main problem with this scenario is that the fluid used by Lerouge *et al.* [8,10,11] to observe the instability most probably belongs to the *stable* region of the stability diagram proposed in [16] (see Supplemental Material [17]), casting doubt on the proposed mechanism.

In this Letter we show that this contradiction is resolved if one relaxes the assumption of axisymmetric flow. We perform a linear stability analysis of the shear-banded Taylor-Couette flow with respect to nonaxisymmetric disturbances for a model fluid with material properties similar to the solutions used in the experiments by Lerouge *et al.* [8,10,11]. We find that while axisymmetric perturbations

are stable as predicted by Fielding [16], nonaxisymmetric modes are unstable for *all* applied shear rates on the stress plateau. The nature of the instability depends on the applied shear rate: very close to the beginning of the plateau, we find this is dominated by the interfacial mode, while most of the plateau is unstable via the bulk mode in agreement with the observations by Fardin *et al.* [11].

Our model consists of the momentum conservation equation in the limit of negligible inertia,

$$-\boldsymbol{\nabla} p + \eta_s \Delta \boldsymbol{v} + \boldsymbol{\nabla} \cdot \boldsymbol{\tau} = \boldsymbol{0}, \tag{1}$$

and the diffusive Johnson-Segalman (DJS) equation [1,15,16,18,19] for the viscoelastic stress $\boldsymbol{\tau}$:

$$\boldsymbol{\tau} + \lambda\left(\frac{1+a}{2}\overset{\triangledown}{\boldsymbol{\tau}} + \frac{1-a}{2}\overset{\triangle}{\boldsymbol{\tau}}\right) - l^2\nabla^2\boldsymbol{\tau} = \eta_p(\boldsymbol{\nabla v} + \boldsymbol{\nabla v}^\dagger), \tag{2}$$

where $\overset{\triangledown}{\boldsymbol{\tau}} = \partial\boldsymbol{\tau}/\partial t + \boldsymbol{v}\cdot\boldsymbol{\nabla\tau} - \boldsymbol{\nabla v}^\dagger\cdot\boldsymbol{\tau} - \boldsymbol{\tau}\cdot\boldsymbol{\nabla v}$ and $\overset{\triangle}{\boldsymbol{\tau}} = \partial\boldsymbol{\tau}/\partial t + \boldsymbol{v}\cdot\boldsymbol{\nabla\tau} + \boldsymbol{\nabla v}\cdot\boldsymbol{\tau} + \boldsymbol{\tau}\cdot\boldsymbol{\nabla v}^\dagger$ are the upper- and lower-convected derivatives, respectively [1]; $(\boldsymbol{\nabla v})_{ij} = \partial v_j/\partial x_i$ is the velocity gradient tensor, and $\dagger$ denotes the transpose. Here, $\boldsymbol{v}$ and p are the velocity and pressure, η_s and η_p are the viscosities of the Newtonian "solvent" and viscoelastic (micellar) components, and λ is the Maxwell relaxation time. The slip parameter a controls the degree of nonaffine deformations under flow [18] and Eq. (2) predicts a nonmonotonic flow curve (shear-banding) as long as $a \neq \pm 1$ and $\eta_p/\eta_s > 8$. The stress-diffusion term $l^2\nabla^2\boldsymbol{\tau}$ in Eq. (2) prevents stress variations on scales smaller than l and uniquely selects the value of the plateau shear stress [19]. The length scale l sets the size of structural correlations in the fluid, and controls the width of the interface between the bands and the extent of the near-wall layers where the bulk behavior changes rapidly in order to match the boundary conditions. Finally, we assume that the fluid is incompressible, $\boldsymbol{\nabla}\cdot\boldsymbol{v} = 0$, and apply the no-slip boundary conditions for the velocity $\boldsymbol{v}$ and the no-flux boundary conditions for the stress tensor $\boldsymbol{\tau}$ [15,16].

We consider the Taylor-Couette flow between two coaxial cylinders. The inner cylinder of radius R_1 rotates with the angular velocity Ω, while the outer cylinder of radius R_2 is kept stationary. The fluid flows in the gap of size $d = R_2 - R_1$ and the relative curvature of the Taylor-Couette cell is set by $\epsilon = d/R_1$. We choose the parameters in our model, Eqs. (1) and (2), to closely match their experimental values as used by Lerouge *et al.* [8,10,11] and set $R_1 = 13.33$ mm and $d = 1.13$ mm. To find the relaxation time λ, the slip parameters a and the viscosities η_s and η_p, we fit the rheological predictions of the Johnson-Segalman model in plane homogeneous shear flow to the cone-and-plate measurements for a solution used in [10].

In Fig. 1 we compare the experimental data (crosses, courtesy of S. Lerouge) against the fit to the Johnson-Segalman model (solid and dashed lines) with

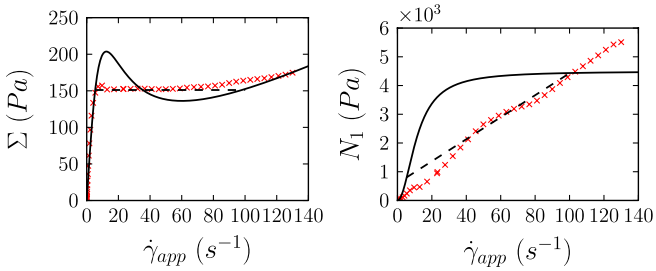

FIG. 1 (color online). Total shear stress Σ and first normal-stress difference N_1 as a function of the applied shear rate $\dot{\gamma}_{\text{app}}$. Crosses—experimental measurements by S. Lerouge *et al.* [10] in a cone-and-plate geometry; solid line—JS constitutive curve for planar homogeneous shear flow; dashed line—prediction of the JS model in planar shear-banded flow.

$\lambda = 0.51$ s, $a = 0.985$, $\eta_s = 1.1$ Pa s and $\eta_p = 33.0$ Pa s. These parameters are similar to the linear rheological measurements of [10], $\lambda \approx 0.23$ s and $\eta_s + \eta_p \approx 55$ Pa s. We mostly consider two values of the structural length scale, $l = 13\ \mu$m and $l = 4\ \mu$m, which are consistent with the experimentally determined values [10,20,21].

First we introduce cylindrical coordinates (r, θ, z) and solve the equations of motion (1) and (2) numerically for the steady 1D shear-banded profile using a pseudospectral Chebyshev-tau method [22]. To accurately resolve sharp interfaces we split the computational domain into three regions, two for each shear band and one corresponding to the interface, and use adaptive domain decomposition algorithm to discretize them independently. A similar method was employed in [23].

The linear stability analysis is performed by perturbing the 1D profile with 3D perturbations of the form $(\boldsymbol{v}, \boldsymbol{\tau}, p) \sim \exp(\sigma t + ikz + im\theta)$, linearizing the equations of motion, and solving the resulting generalized eigenvalue problem. Below, the applied shear rate is reported in terms of the dimensionless Weissenberg number $\text{Wi} = \lambda\Omega/[\epsilon(\epsilon + 2)]$.

In Fig. 2 we plot the real part of the most unstable eigenvalue σ^* and the corresponding wavelengths k^* and

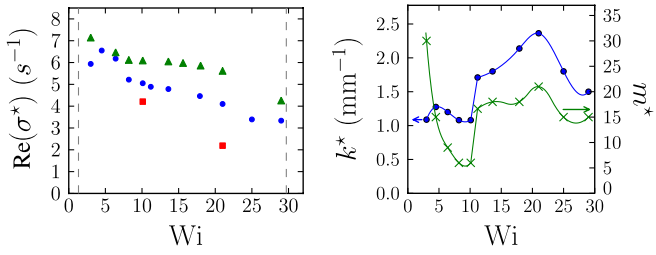

FIG. 2 (color online). (left) Maximum growth rate $\text{Re}(\sigma^\star)$ as a function of Wi on the stress plateau (boundaries denoted by the dashed lines) for various values of the diffusion length l: squares—$l = 73\ \mu$m, circles—$l = 13\ \mu$m, triangles—$l = 4\ \mu$m. (right) Axial and azimuthal wavelengths k^* and m^* of the most unstable mode as a function of Wi for $l = 13\ \mu$m. The lines are drawn to guide the eye.

m^* as a function of Wi. We find that the shear-banded profile is unstable on the whole plateau, contrary to the *axisymmetric* prediction for our parameters [16].

In order to determine whether the instability is interfacial or bulk, we employ the following method. For every Wi along the stress plateau, we construct an auxiliary Taylor-Couette system that models only the high-shear-rate band of the original flow. The flow in the auxiliary system is homogeneous (not shear-banded) and has the same laminar velocity and stress profiles as the original high-shear-rate band. This is achieved by choosing the gap size of the auxiliary flow cell to be equal to the width of the high-shear-rate band and rotating both inner and outer cylinders, while keeping R_1 and the DJS parameters the same as above. As the result, the high-shear-rate band and its model version only differ in the nature of their outer boundary—the interface with the low-shear-rate band (soft) or a wall (hard), respectively. (For a recent discussion of the soft vs hard boundary conditions in the context of shear-banding; see [24].) We then compare the eigenspectra in both setups: the eigenmodes that appear in both systems clearly correspond to the bulk instability. No instability was found when the same procedure was applied to the low-shear-rate band.

In Fig. 3(a) we show the comparison of the shear-banded and (homogeneous) auxiliary systems at Wi = 29 (near the upper end of the stress plateau) for k^* and m^*, the most unstable values of k and m. In Fig. 3(c) we present the contour plot of the real part of the leading eigenvalue for different values of k and m in both setups. In spite of the different boundary conditions in the two systems, we observe that their leading eigenvalues coincide, which we attribute to the small size of the low-shear-rate band at high Wi and the influence of the no-slip boundary condition at the wall on the high-shear-rate band. This coincidence implies that the instability originates in the bulk of the high-shear-rate band. Moreover, we find no local maxima besides the eigenvalue family corresponding to the most unstable bulk mode, which is dominant in a wide range of Wi $\sim$ 10–30. The fact that we see a 3D instability where the axisymmetric analysis predicted stable flow [16], is perhaps not surprising since the first instability predicted for purely elastic Taylor-Couette flow of polymer solutions, which is similar to our bulk instability, is non-axisymmetric [25].

For small values of the applied shear rate the situation is different. As can be seen from Fig. 3(b) for Wi = 3.0, the most unstable mode of the shear-banded profile does not coincide with any eigenvalue of the auxiliary system, and we conclude that this instability is driven by the interface. We also observe, Fig. 3(d), that the shape of this eigenvalue family on the Re$\sigma(k, m)$ contour plot is different from the bulk mode of Fig. 3(c), and is similar to what was found by Fielding for the interfacial mode in plane shear [15].

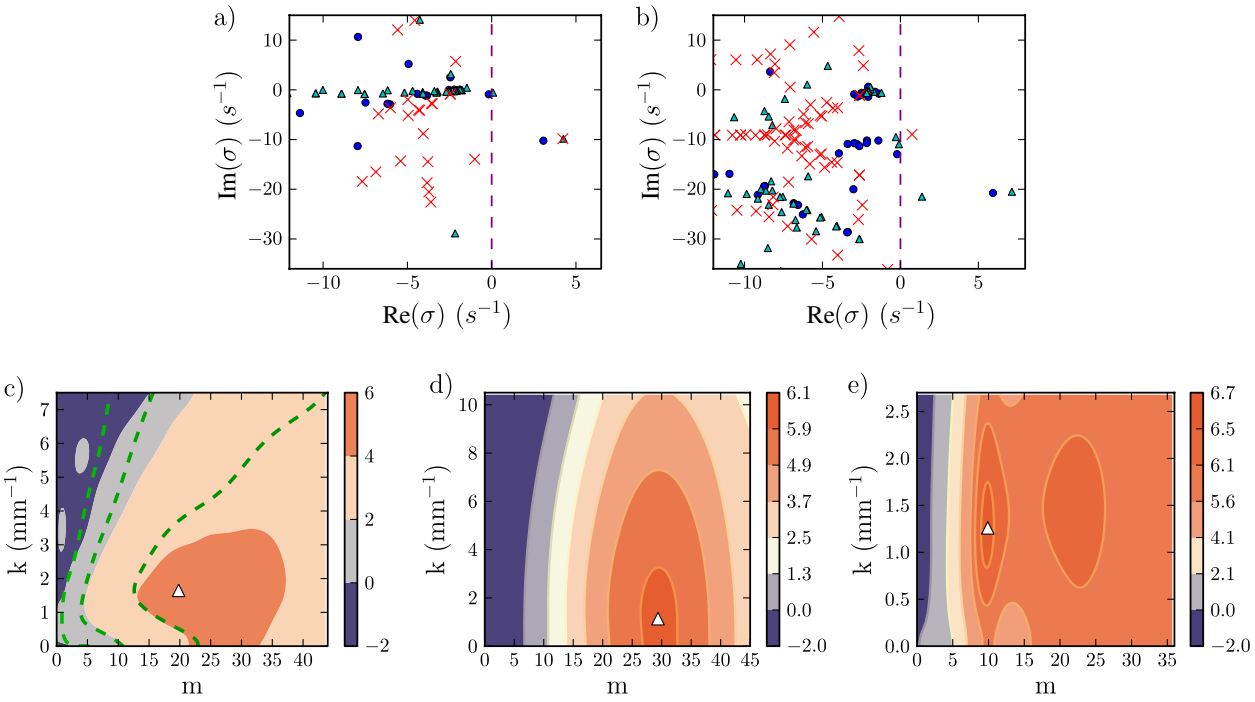

FIG. 3 (color online). (top) Superimposed spectra showing the most unstable eigenvalue for the shear-banded (dots—$l = 13$ μm, triangles—$l = 4$ μm) and the auxiliary (crosses—$l = 4$ μm) setup. (a) Wi = 29, $k = 20.54$ and $m = 21$; (b) Wi = 3.0, $k = 14.4$ and $m = 30$. (bottom) Contour plots of the dispersion relation Re$\sigma(k, m)$ as a function of m and k. White triangle marks the most unstable eigenmode. (c) Wi = 29 and $l = 4$ μm, green dashed lines—contour plot for the auxiliary system; (d) Wi = 3.0 and $l = 13$ μm; (e) Wi = 6.4 and $l = 4$ μm showing two types of instability.

At intermediate values of the applied shear rate, both the interfacial and bulk modes are unstable, as can be seen from Fig. 3(e). The velocity profiles corresponding to the two peaks in the Re$\sigma(k, m)$ contour plot differ fundamentally: one has its maximum velocity in the vicinity of the interface, while the other is mostly present in the bulk (see Supplemental Material [17]). The height of the bulk peak rapidly overtakes that of the interfacial peak as Wi is increased. The transition from the interfacial to the bulk mode takes place at the critical value of the Weissenberg number that depends on the diffusive length: $\mathrm{Wi}_{\mathrm{crit}} \approx 10$ for $l = 13$ μm, and $\mathrm{Wi}_{\mathrm{crit}} \approx 6$–$8$ for $l = 4$ μm.

Our use of the auxiliary Taylor-Couette systems to determine the nature of the instability is motivated by the observation that decreasing the value of the diffusion length l enhances *both* modes of instability. Indeed, this parameter not only controls the width of the interface, thus affecting the interfacial mode [15], but also sets the minimal spatial extent of stress gradients in the fluid, and hence has a strong effect on the bulk mode as well. Therefore, one cannot deduce the nature of an eigenmode by observing how its eigenvalue changes with l.

In summary, we presented theoretical evidence that the shear-banded Taylor-Couette flow is unstable with respect to nonaxisymmetric perturbations. For parameters matched to the experiments by Lerouge *et al.* [8,10,11], we find the interfacial instability only at the beginning of the stress plateau, while most of the plateau is occupied by the bulk instability. These results are consistent with the observations by Fardin *et al.* [11], where the Taylor vortices, localized mostly in the high-shear-rate band, were observed in a wide range of shear rates on the stress plateau. Moreover, we find instabilities with the axial wavelengths of order of a few millimeters, roughly in agreement with the asymptotic (nonlinear) wavelengths observed by Lerouge *et al.* [10]. Potentially, our prediction is further supported by recent experiments of Decruppe *et al.* [26], who observed *azimuthal* undulations of the interface. However, unlike [8,10,11], no axial interface perturbations were found in their experiment, and its relevance to our work remains an open question.

As was noted by Fielding [16], the Taylor-Couette flow of wormlike micellar solutions is unique as it brings together three types of instabilities: shear banding itself and the interfacial and bulk ones. The stability diagram proposed in [16], based on the axisymmetric analysis, included regions of interfacial and bulk instabilities separated by a window of stable shear-banded flow, and any given micellar solution was predicted to belong to only one of these regions. Our results, based on the nonaxisymmetric linear stability analysis, suggest that both types of instabilities can be found for a given micellar solution. We speculate that the whole curvature-N_1 stability diagram may be occupied by the unstable region, with the position of the transition between the interfacial and bulk modes, $\mathrm{Wi}_{\mathrm{crit}}$, being determined by the normal stresses in the high-shear-rate band: for larger values of N_1 the transition would happen at smaller $\mathrm{Wi}_{\mathrm{crit}}$.

We would like to thank Sandra Lerouge for providing the rheological data used in Fig. 1, and Mike Cates, Marc Fardin, and Sandra Lerouge for useful discussions. A. M. acknowledges support from the EPSRC Career Acceleration Fellowship (grant EP/I004262/1).

*Alexander.Morozov@ph.ed.ac.uk

[1] R. G. Larson, *The Structure and Rheology of Complex Fluids* (Oxford University Press, Oxford, 1999).
[2] M. E. Cates and S. M. Fielding, Adv. Phys. **55**, 799 (2006); S. Lerouge and J.-F. Berret, Adv. Polym. Sci. **230**, 1 (2010).
[3] P. Schall and M. van Hecke, Annu. Rev. Fluid Mech. **42**, 67 (2010).
[4] C. Gilbreth, S. Sullivan, and M. Dennin, Phys. Rev. E **74**, 051406 (2006).
[5] L. B. Chen *et al.*, Phys. Rev. Lett. **69**, 688 (1992); R. Besseling *et al.*, *ibid.* **105**, 268301 (2010).
[6] H. Rehage and H. Hoffmann, Mol. Phys. **74**, 933 (1991).
[7] M. E. Cates, J. Phys. Condens. Matter **8**, 9167 (1996).
[8] S. Lerouge, M. Argentina, and J. P. Decruppe, Phys. Rev. Lett. **96**, 088301 (2006).
[9] L. Becu *et al.*, Phys. Rev. E **76**, 011503 (2007).
[10] S. Lerouge *et al.*, Soft Matter **4**, 1808 (2008).
[11] M. A. Fardin *et al.*, Phys. Rev. Lett. **103**, 028302 (2009).
[12] Y. Renardy, J. Non-Newtonian Fluid Mech. **28**, 99 (1988); E. J. Hinch *et al.*, *ibid.* **43**, 311 (1992); Y. Renardy and M. Renardy, *ibid.* **81**, 215 (1999).
[13] R. G. Larson *et al.*, J. Fluid Mech. **218**, 573 (1990).
[14] P. Pakdel and G. H. McKinley, Phys. Rev. Lett. **77**, 2459 (1996).
[15] S. M. Fielding, Phys. Rev. Lett. **95**, 134501 (2005); S. M. Fielding and P. D. Olmsted, *ibid.* **96**, 104502 (2006); H. J. Wilson and S. M. Fielding, J. Non-Newtonian Fluid Mech. **138**, 181 (2006); S. M. Fielding, Phys. Rev. E **76**, 016311 (2007).
[16] S. M. Fielding, Phys. Rev. Lett. **104**, 198303 (2010).
[17] See Supplementary Materials at http://link.aps.org/supplemental/10.1103/PhysRevLett.108.088302 for details.
[18] M. W. Johnson and D. Segalman, J. Non-Newtonian Fluid Mech. **2**, 255 (1977).
[19] P. D. Olmsted *et al.*, J. Rheol. **44**, 257 (2000).
[20] P. Ballesta *et al.*, J. Rheol. **51**, 1047 (2007); C. Masselon *et al.*, Phys. Rev. Lett. **100**, 038301 (2008).
[21] M. A. Fardin *et al.*, Phys. Rev. Lett. **104**, 178303 (2010).
[22] C. Canuto, M. Hussaini, A. Quarteroni, and T. Zang, *Spectral Methods in Fluid Dynamics* (Springer Verlag, New York, 1988).
[23] M. Cromer *et al.*, J. Non-Newtonian Fluid Mech. **166**, 566 (2011).
[24] M. A. Fardin *et al.*, Europhys. Lett. **96**, 44 004 (2011).
[25] M. Avgousti and A. N. Beris, J. Non-Newtonian Fluid Mech. **50**, 225 (1993).
[26] J. P. Decruppe *et al.*, Phys. Rev. Lett. **105**, 258301 (2010).